Crystal structure and magnetic properties of 6*H*-$SrMnO_3$

Alexei A. Belik,[1,*] Yoshitaka Matsushita,[2] Yoshio Katsuya,[3] Masahiko Tanaka,[2] Taras Kolodiazhnyi,[4] Masaaki Isobe,[4] and Eiji Takayama-Muromachi[1]

[1]*International Center for Materials Nanoarchitectonics (MANA), National Institute for Materials Science (NIMS), 1-1 Namiki, Tsukuba, Ibaraki 305-0044, Japan*

[2]*SPring-8 Office, NIMS, Kohto 1-1-1, Sayo-cho, Hyogo 679-5148, Japan*

[3]*SPring-8 Service Co., Ltd., 1-1-1 Kouto, Sayo-cho, Hyogo 679-5148, Japan*

[4]*Superconducting Materials Center (SMC), NIMS, 1-1 Namiki, Tsukuba, Ibaraki 305-0044, Japan*

(Received 17 May 2011; published 22 September 2011)

The 6*H*-$SrMnO_3$ polymorph was prepared using a high-pressure and high-temperature technique at 6 GPa and 1773 K. Its crystal structure was refined using synchrotron x-ray powder diffraction data (space group $P6_3/mmc$ (no. 194), $Z = 6$, $a = 5.42892(1)$ Å, $c = 13.40252(3)$ Å). Magnetic and transport properties of 6*H*-$SrMnO_3$ were investigated using direct current magnetization, specific heat, and resistivity measurements. The antiferromagnetic Néel temperature T_N of 6*H*-$SrMnO_3$ is 235 K; this value is close to that of cubic-$SrMnO_3$ ($T_N = 240$ K) and 4*H*-$SrMnO_3$ ($T_N = 280$ K). 6*H*-$SrMnO_3$ and 4*H*-$SrMnO_3$ have the same building blocks of face-sharing MnO_6 octahedra. Magnetic susceptibility of 6*H*-$SrMnO_3$ exhibits behavior typical for classical three-dimensional antiferromagnets with a maximum near T_N—in contrast to those of cubic-$SrMnO_3$ and 4*H*-$SrMnO_3$, where broad maxima are observed far above T_N. Isothermal magnetization curves of 6*H*-$SrMnO_3$ (at 2 K) show an upturn deviation from the linear behavior above 10 kOe, indicating a possible spin–flop magnetic phase transition.

DOI: 10.1103/PhysRevB.84.094438 PACS number(s): 75.50.Ee, 75.40.Cx, 61.05.cp

I. INTRODUCTION

$AMnO_3$ (A = Ca, Sr, and Ba) compounds have been extensively studied because of their interesting electronic, magnetic, and structural properties.[1–17] Most recently, attention has focused on multiferroic behavior[1] and interfacial properties of thin films.[2] $CaMnO_3$ crystallizes in the $GdFeO_3$-type perovskite structure (space group $Pnma$, $Z = 4$, $a = 5.2770$ Å, $b = 7.4510$ Å, $c = 5.2643$) with corner-sharing MnO_6 octahedra [Fig. 1(a)]. Its antiferromagnetic (AFM) Néel temperature T_N is 125 K.[3]

$BaMnO_3$ adopts a 2*H* hexagonal structure (space group $P6_3/mmc$, $Z = 2$, $a = 5.6991$ Å, $c = 4.8148$) with face-sharing MnO_6 octahedra [Fig. 1(b)].[4,5] Hereafter, *H* stands for a hexagonal system, and a numeral indicates a number of the layers in a unit cell.[18] Reported magnetic properties of stoichiometric 2*H*-$BaMnO_3$ are rather controversial.[4,5] In contrast to the stoichiometric $BaMnO_3$, oxygen-deficient $BaMnO_{3-\delta}$ adopts different hexagonal/rhombohedral structures with variable ratios of corner-sharing (cubic) and face-sharing (hexagonal) layers.[6,7] Using a high-pressure, high-temperature (HPHT) method, the 4*H* and 9*R* (*R* means a rhombohedral system)[18] polymorphs of stoichiometric $BaMnO_3$ can be achieved.[8,9]

Stoichiometric $SrMnO_3$ is known to form three polymorphs: 4*H*- [Fig. 1(c)] and 6*H*-hexagonal and cubic (*C*) perovskite [Fig. 1(a)].[8–12] Electronic, magnetic, and structural properties of 4*H*-$SrMnO_3$ and *C*-$SrMnO_3$ are well known. The T_N of 4*H*-$SrMnO_3$ (space group $P6_3/mmc$, $Z = 4$, $a = 5.454$ Å, $c = 9.092$ Å) is ∼280 K.[11] Above the Néel temperature, 4*H*-$SrMnO_3$ shows a broad anomaly in magnetic susceptibility due to short-range AFM interactions between the Mn^{4+} ions in the face-sharing MnO_6 octahedra. This high-temperature anomaly was the reason for the erroneously reported $T_N = 350$ K in the early studies.[8] *C*-$SrMnO_3$ (space group $Pm\text{–}3m$, $Z = 1$, $a = 3.8041$ Å) adopts a G-type AFM structure below $T_N = 230$–260 K.[12–14] The variation in T_N is probably due to small variations in the oxygen stoichiometry. Oxygen nonstoichiometric $SrMnO_{3-\delta}$ samples have also been extensively investigated in Refs. 19–21.

6*H*-$SrMnO_3$ can be prepared using the HPHT method.[8,9] However, this polymorph was basically unexplored. To the best of our knowledge, very limited or no structural information is available in the standard databases and/or main journals, and it was suggested that the T_N of 6*H*-$SrMnO_3$ is probably 90 K.[8]

In this work, we investigated the crystal structure of 6*H*-$SrMnO_3$ using synchrotron x-ray powder diffraction (XRD) data. Magnetic properties of 6*H*-$SrMnO_3$ were clarified and compared with those of 4*H*-$SrMnO_3$ and *C*-$SrMnO_3$. The T_N of 6*H*-$SrMnO_3$ was determined to be 235 K. Magnetic susceptibilities of 6*H*-$SrMnO_3$ are typical for classical antiferromagnets with a maximum near T_N—compared to those of *C*-$SrMnO_3$ and 4*H*-$SrMnO_3$, where broad maxima are observed far above T_N. The isothermal magnetization curves of 6*H*-$SrMnO_3$ (at 2 K) show an upturn deviation from the linear behavior above 10 kOe.

II. EXPERIMENT

A single-phase 4*H*-$SrMnO_3$ powder sample [Fig. 2(b)], with refined lattice parameters of $a = 5.4487(1)$ Å and $c = 9.0791(1)$ Å, was prepared from a stoichiometric mixture of $SrCO_3$ and Mn_2O_3 by firing in air at 1423 K for 50 h, followed by annealing at 1273 K for 24 h, and finally by cooling to room temperature (RT) in 2 h. The oxygen content of the 4*H*-phase was determined to be $SrMnO_{2.99(2)}$ from the weight loss after reduction at 1273 K for 3 h in the flow of 100% H_2. The reduction experiments were performed in a tube furnace; the sample weights were measured using a Mettler Toledo XP205 balance before and right after the reduction. 4*H*-$SrMnO_3$ was pelletized with a small amount of polyvinyl alcohol as a binder and fired at 1273 for 55 h. Pellets of a single-phase *C*-$SrMnO_3$ sample [Fig. 2(a)] with the refined lattice parameter of

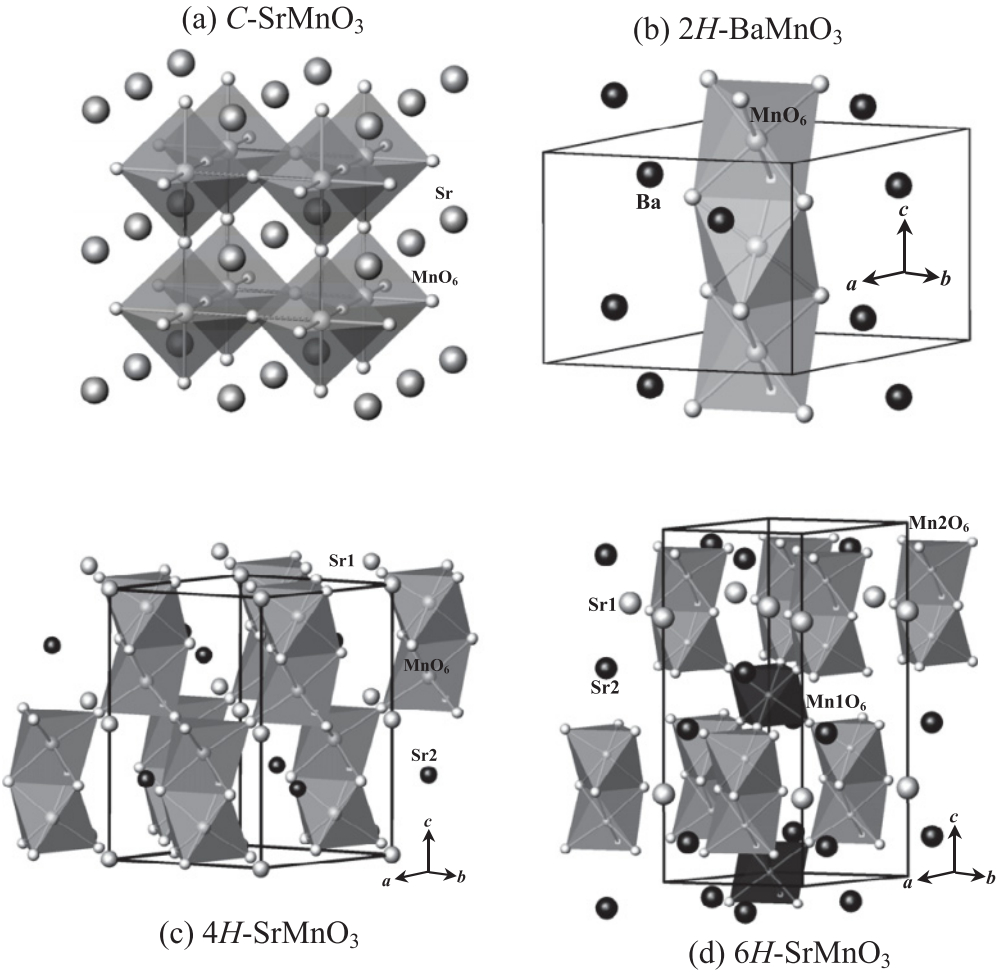

FIG. 1. Polyhedral MnO_6 presentation of the $AMnO_3$ structures: (a) the cubic perovskite C-$SrMnO_3$ with all corner-sharing MnO_6 octahedra, (b) $2H$-$BaMnO_3$ with face-sharing MnO_6 octahedra, (c) $4H$-$SrMnO_3$, and (d) $6H$-$SrMnO_3$. Sr and Ba atoms are shown as spheres.

$a = 3.80564(1)$ Å were prepared from the pellets of $4H$-$SrMnO_3$ in two steps. During the first step, $4H$-$SrMnO_3$ was annealed at 1773 K for 8 h in an Ar flow with the heating/cooling rate of 300 K/h. The weight loss after the first step gave the composition of $SrMnO_{2.53(2)}$. During the second step, the obtained $SrMnO_{2.53}$ sample was oxidized in air at 623 K for 15 h. The weight gain after the second step gave the composition of C-$SrMnO_{2.99(2)}$. $SrMnO_{2.53}$ and C-$SrMnO_{2.99}$ were also heated in air up to 1273 K to check their oxygen content; the weight changes gave the initial compositions of $SrMnO_{2.54(2)}$ and C-$SrMnO_{2.99(2)}$, respectively, assuming that the final oxidized composition is $4H$-$SrMnO_{2.99}$. All weight changes were controlled by the aforementioned balance. The synthesis of $6H$-$SrMnO_3$ was performed from the $4H$-$SrMnO_3$ precursor in a belt-type high-pressure apparatus at 6 GPa and 1700 K for 40 min in sealed Pt capsules. After heat treatment, the samples were quenched to RT, and the pressure was slowly released. No weight change was detected during the preparation of $6H$-$SrMnO_3$. $6H$-$SrMnO_3$ contained traces of the $SrCO_3$ impurity [Fig. 2(c)]. The oxygen content of the $6H$-phase was determined to be $SrMnO_{3.01(2)}$ from the weight loss after its reduction at 1273 K for 3 h in the flow of 100% H_2.

Densities of the samples were determined by the weight changes of the samples in air and in CCl_4. The density of CCl_4 was taken as 1.587 g/cm^3 and confirmed by the density measurement of Pt.

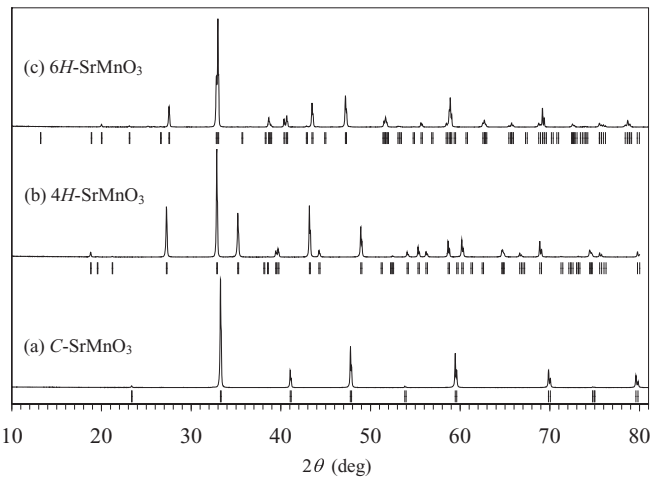

FIG. 2. XRD patterns (measured with CuKα radiation at RT) of (a) C-$SrMnO_3$, (b) $4H$-$SrMnO_3$, and (c) $6H$-$SrMnO_3$. Possible Bragg reflections are indicated by tick marks.

XRD data were collected at RT on a Rigaku Ultima III diffractometer using Cu$K\alpha$ radiation (2θ range of 4–100°, step width of 0.02°, and counting time of 2–10 s/step). Synchrotron XRD data of 6*H*-$SrMnO_3$ were measured at RT on a large Debye-Scherrer camera at the BL15XU beam line of SPring-8.[22] The data were collected between 2° and 60° at the 0.003° interval in 2θ. Incident beam was monochromatized at λ = 0.65297 Å. The sample was packed into a Lindemann glass capillary (inner diameter of 0.1 mm), which was rotated during the measurement. The Rietveld analysis was performed with RIETAN-2000.[23] The weight fraction of the $SrCO_3$ impurity was estimated to be 0.7% based on the refined scale factors of the Rietveld analysis. Anisotropic broadening of reflections was observed in high-resolution synchrotron XRD data, and anisotropic broadening parameters were refined.

Direct current (DC) magnetic susceptibilities χ = **M/H** were measured on a superconducting quantum interference device magnetometer (Quantum Design MPMS) between 2 and 400 K in applied fields of 1 and 10 kOe under both zero-field-cooled (ZFC) and field-cooled (FC; on cooling) conditions. Isothermal magnetization measurements were performed from 70 to −70 kOe and from −70 to 70 kOe at 2 K. The C_p measurements were performed at 0 and 70 kOe on cooling by a pulse relaxation method using a commercial calorimeter (Quantum Design PPMS). To make a good thermal contact between a sample and a holder, the N- and H-type Apiezon greases were used for the 2–300 and 200–390 K temperature intervals, respectively. No detectable differences were observed between the C_p curves measured at 0 and 70 kOe. DC electrical resistivity of 6*H*-$SrMnO_3$ was measured between 10 and 400 K by the conventional four-probe method using a Quantum Design PPMS with the DC-gage current of 10 mA. The DC-gage current was reduced automatically at low temperatures to allow the high resistivity measurements. Resistivity became too high to be measured with our system below ∼230 K.

III. RESULTS AND DISCUSSION

The structure parameters of 6*H*-$BaTiO_{3-\delta}$[24] were used as the initial ones for the refinement of 6*H*-$SrMnO_3$. The refined structural parameters, *R* values, selected bond lengths, and bond valence sums[25] of 6*H*-$SrMnO_3$ are listed in Table I. Experimental, calculated, and difference synchrotron XRD profiles are shown in Fig. 3. The crystal structure of 6*H*-$SrMnO_3$ is shown in Fig. 1(d). The bond valence sum values of +4.11 for Mn1 and +4.09 for Mn2 support the oxidation state of the manganese ions. Density of 6*H*-$SrMnO_3$ (d_{exp} = 5.55(2) g/cm^3 and d_{calc} = 5.550 g/cm^3) is larger than that of 4*H*-$SrMnO_3$ (d_{exp} = 5.43(2) g/cm^3 and d_{calc} = 5.422 g/cm^3). This explains why 6*H*-$SrMnO_3$ is stabilized at high-pressure conditions. However, the density of *C*-$SrMnO_3$ (d_{exp} = 5.67(2) g/cm^3 and d_{calc} = 5.741 g/cm^3) is even larger. *C*-$SrMnO_3$ can be considered a metastable phase, which was prepared by low-temperature oxidation. This is why this densest polymorph is not formed at HPHT conditions.

Figures 4 and 5 show DC magnetic susceptibilities of 4*H*-$SrMnO_3$ and 6*H*-$SrMnO_3$ and of *C*-$SrMnO_3$, respectively. 4*H*-$SrMnO_3$ and *C*-$SrMnO_3$ demonstrate very broad maxima above T_N, in agreement with previous reports.[8,14] Therefore,

TABLE I. Structure parameters, bond lengths, and bond valence sums of 6*H*-$SrMnO_3$ at RT.

Site	Wyckoff position	*x*	*y*	*z*	*B* (Å^2)
Sr1	2*b*	0	0	0.25	0.28(3)
Sr2	4*f*	1/3	2/3	0.08938(5)	0.262(14)
Mn1	2*a*	0	0	0	0.35(4)
Mn2	4*f*	1/3	2/3	0.84369(6)	0.07(2)
O1	6*h*	0.5132(3)	=2*x*	0.25	0.10(7)
O2	12*k*	0.8353(3)	=2*x*	0.08125(16)	0.59(4)

[1]*Note*. Space group is $P6_3/mmc$ (no. 194), $Z = 6$, $a = 5.42892(1)$ Å, $c = 13.40252(3)$ Å, and $V = 342.0929(9)$ Å^3. *R* values are $R_{wp} = 2.04\%$, $R_p = 1.11\%$, $R_B = 3.05\%$, $R_F = 2.42\%$, and $R_{exp} = 0.21\%$ (a very small value of R_{exp} is an artifact due to a large number of experimental points). The weight fraction of the impurity $SrCO_3$ was 0.7%. The occupation factor *g* of all the sites is unity ($g = 1$). Densities are d_{exp} = 5.55(2) g/cm^3 and d_{calc} = 5.550 g/cm^3. d(Mn1-O2) = 1.893(3) Å × 6, d(Mn2-O2) = 1.878(3) Å × 3, d(Mn2-O1) = 1.913(2) Å × 3. d(Sr1-O1) = 2.7173(1) Å × 6, d(Sr1-O2) = 2.741(3) Å × 6, d(Sr2-O1) = 2.737(2) Å × 3, d(Sr2-O2a) = 2.7167(1) Å × 6, d(Sr2-O2b) = 2.783(3) Å × 3. d(Mn2-Mn2) = 2.511(2) Å. BVS(Mn1) = +4.11, BVS(Mn2) = +4.09, BVS(Sr1) = +2.30, and BVS(Sr2) = +2.25; BVS = $\sum_{i=1}^{N} v_i$, $v_i = \exp[(R_0 - d_i)/B]$, where BVS is the bond valence sum, *N* is the coordination number, B = 0.37, $R_0(Mn^{4+})$ = 1.753, $R_0(Sr^{2+})$ = 2.118, and d_i is the bond length (Ref. 25).

T_N of these phases can be defined by a peak position on the differential FC $d\chi/dT$ vs T curves. This yields T_N = 280 K for 4*H*-$SrMnO_3$ and T_N = 240 K for *C*-$SrMnO_3$ (the measurement step was 5 K in this temperature range). These values are in good agreement with previous reports.[11–14] Magnetic susceptibilities of 6*H*-$SrMnO_3$ exhibit a rather sharp maximum near T_N = 235 K, which is typical for classical antiferromagnets. The ZFC and FC $d\chi/dT$ vs T curves of 6*H*-$SrMnO_3$ also show peaks at T_N. In contrast to 4*H*-$SrMnO_3$ and *C*-$SrMnO_3$, magnetic susceptibilities of 6*H*-$SrMnO_3$ above T_N follow the Curie-Weiss law [Fig. 4(b)]. The fitting to the Curie-Weiss law $\chi = \mu_{eff}{}^2/[8(T - \theta)]$ between 330 and 400 K yields the effective magnetic moment μ_{eff} of 4.099(6)μ_B

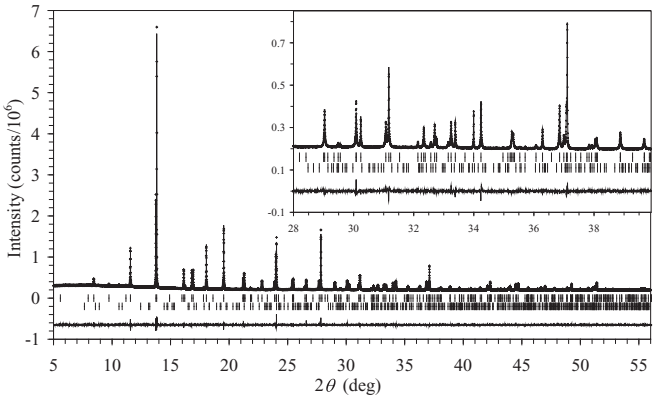

FIG. 3. Portions of experimental (crosses), calculated (lines), and difference synchrotron (λ = 0.65297 Å) XRD patterns for 6*H*-$SrMnO_3$. Bragg reflections are indicated by tick marks: The first row is for 6*H*-$SrMnO_3$, and the second row is for the $SrCO_3$ impurity (0.7 weight%). The inset gives an enlarged fragment.

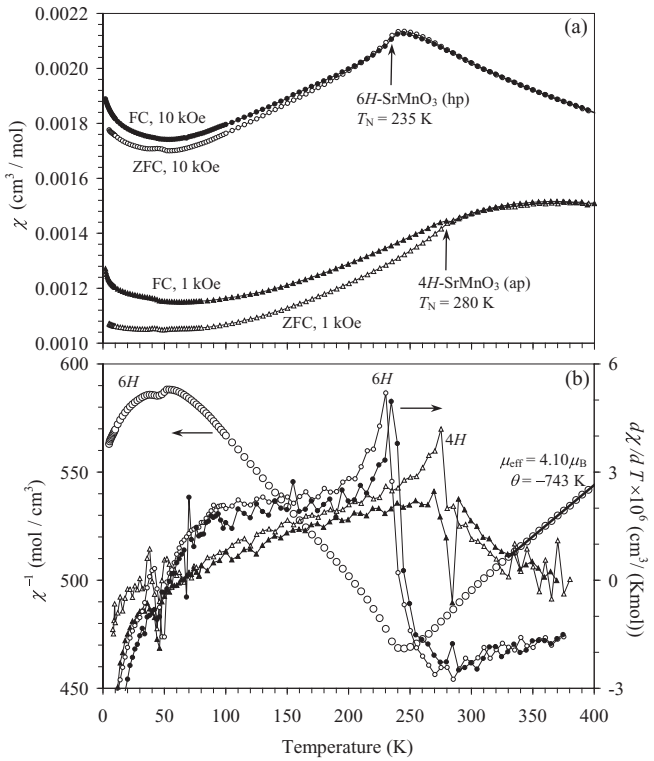

FIG. 4. (a) ZFC (white symbols) and FC measured on cooling (black symbols) DC magnetic susceptibility (χ = **M/H**) curves of $4H$-$SrMnO_3$ measured at 1 kOe (triangles) and $6H$-$SrMnO_3$ measured at 10 kOe (circles). Arrows show the AFM Néel temperatures T_N, ap indicates the ambient-pressure phase, and hp indicates the high-pressure phase. (b) The ZFC inverse magnetic susceptibilities of $6H$-$SrMnO_3$ and the ZFC and FC $d\chi/dT$ vs T curves of $4H$-$SrMnO_3$ and $6H$-$SrMnO_3$. The linear curve between 330 and 400 K depicts the Curie-Weiss fit, with the fitting parameters given in the figure.

and the Curie-Weiss constant θ of $-743(3)$ K. The ratio $|\theta\ /\ T_N| \approx 3.2$ indicates the presence of frustration. The μ_{eff} is closer to the expected value of $3.87\mu_B$ for Mn^{4+} ($S = 3/2$) than to the reported values for $CaMnO_3$ ($\mu_{eff} = 4.34\mu_B$)[3] and $4H$-$SrMnO_3$ ($\mu_{eff} = 4.6\mu_B$).[8] Our own data on $CaMnO_3$ gave

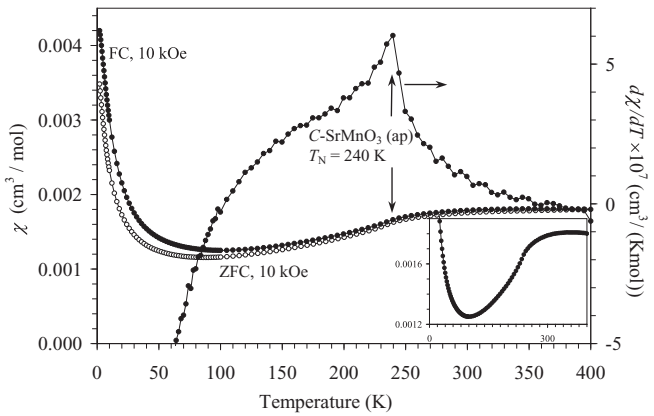

FIG. 5. ZFC (white circles) and FC measured on cooling (black circles) DC magnetic susceptibility curves of C-$SrMnO_3$ measured at 10 kOe. The right-hand axis gives the FC $d\chi/dT$ vs T data for C-$SrMnO_3$. Arrows show T_N. The inset gives the enlarged FC curve.

$\mu_{eff} = 4.30\mu_B$ and $\theta = -478$ K. Very weak anomalies observed near 45–50 K (especially on the ZFC curves) in $4H$-$SrMnO_3$ and $6H$-$SrMnO_3$ [Fig. 4] probably originate from undetectable (by XRD) traces of the ferrimagnetic Mn_3O_4 impurity with $T_C = 43$ K.

Previous works showed that $BaMnO_3$ does not follow the Curie-Weiss law up to 300 K.[4] Magnetic susceptibilities of $2H$-$BaMnO_3$ show a broad anomaly near 150 K and no anomalies at $T_N = 59$ K.[4] The broad anomaly is usually explained by the one-dimensional [Fig. 1(b)] short-range AFM ordering. The absence of an anomaly near T_N is explained by the three-dimensional order being developed from the one-dimensional order; therefore, there is no reduction in the magnetic susceptibility.[4]

The broad anomaly (near 350 K) above T_N in magnetic susceptibilities of $4H$-$SrMnO_3$ is usually explained by the short-range AFM interactions between the Mn^{4+} ions in the face-sharing MnO_6 octahedra [Fig. 1(c)].[13] C-$SrMnO_3$ with a three-dimensional structure [Fig. 1(a)] should exhibit properties typical for the three-dimensional isotropic antiferromagnets (as in the case of $CaMnO_3$),[3] as well as the highest T_N.[6] However, this is not the case, and C-$SrMnO_3$ demonstrates broad anomalies above T_N, similar to $4H$-$SrMnO_3$. These magnetic peculiarities of C-$SrMnO_3$ remain unexplained to the best of our knowledge. Competitions between the nearest-neighbor interaction provided by the 180° Mn-O-Mn path and the next-nearest-neighbor interactions may be responsible for the anomalous magnetic behavior of C-$SrMnO_3$.

In contrast to C-$SrMnO_3$, $6H$-$SrMnO_3$ has face-sharing dimer units in its structure [Fig. 1(d)] similar to $4H$-$SrMnO_3$; therefore, it should exhibit low-dimensional magnetic features. Surprisingly, $6H$-$SrMnO_3$ behaves essentially as a classical three-dimensional isotropic antiferromagnet with the Curie-Weiss behavior above T_N. In the case of $BaMnO_{3-\delta}$, it was shown that the samples with a larger fraction of cubic layers within the structure have higher T_N.[6] This tendency is not obeyed for $SrMnO_3$, where $6H$-$SrMnO_3$ with more cubic layers within its structure has lower T_N compared to $4H$-$SrMnO_3$. Therefore, theoretical studies and evaluation of the

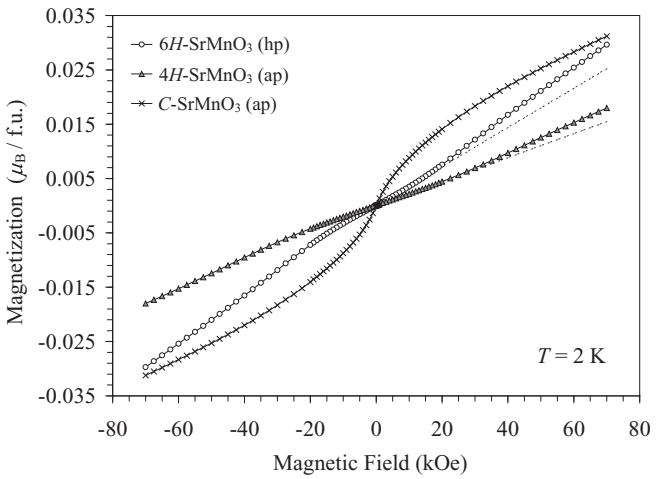

FIG. 6. Isothermal magnetization curves of C-$SrMnO_3$ (black crosses), $4H$-$SrMnO_3$ (gray triangles), and $6H$-$SrMnO_3$ (white circles) at 2 K from 70 to -70 kOe. No detectable differences were observed in the curves measured from -70 to 70 kOe.

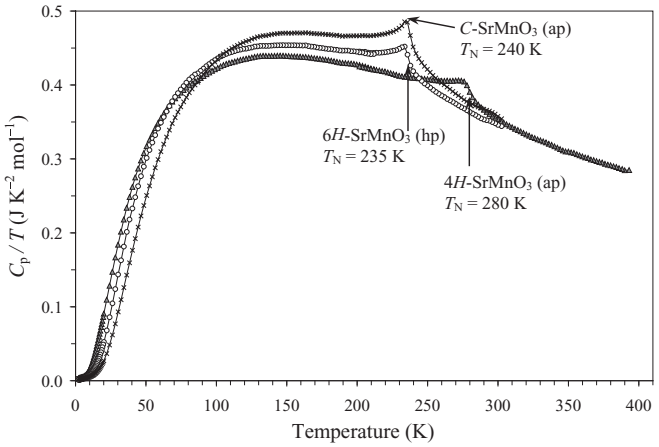

FIG. 7. C_p/T vs T curves for C-$SrMnO_3$ (black crosses), 4H-$SrMnO_3$ (gray triangles), and 6H-$SrMnO_3$ (white circles) at 0 Oe. Arrows show T_N determined from the FC $d\chi/dT$ vs T curves.

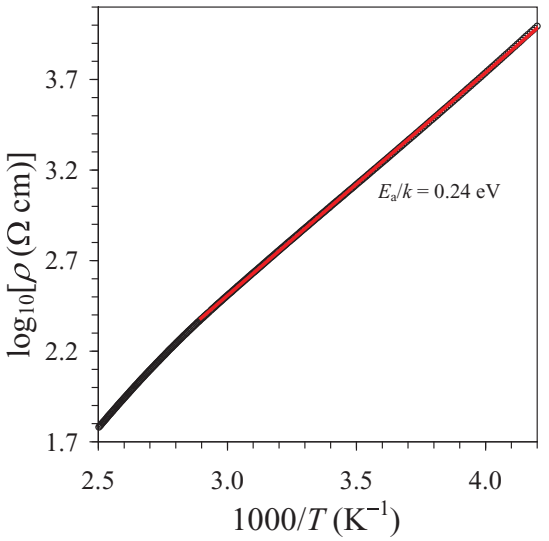

FIG. 8. (Color online) The $\log_{10}(\rho)$ vs $10^3/T$ curve for 6H-$SrMnO_3$. The line shows the fit to the activation law.

strengths of different Mn-O-Mn and Mn-O-O-Mn interactions and the experimental determination of magnetic structures and ordered magnetic moments will be helpful for understanding the differences among the three polymorphs of $SrMnO_3$.

Figure 6 depicts the isothermal magnetization curves of C-$SrMnO_3$, 4H-$SrMnO_3$, and 6H-$SrMnO_3$ measured at 2 K. No hysteresis was observed in all three polymorphs, in agreement with their AFM ground states. The **M** vs **H** curves of 6H-$SrMnO_3$ and 4H-$SrMnO_3$ are linear up to 10 and 22 kOe, respectively. Above these fields, upturn deviations from the linear behavior were observed, indicating a magnetic field–induced transition. C-$SrMnO_3$ shows a downturn deviation at higher magnetic fields from the initial linear behavior. The magnetic moment reaches only $\sim 0.03\mu_B$ per formula unit at 70 kOe for 6H-$SrMnO_3$ and C-$SrMnO_3$ and $0.018\mu_B$ per formula unit for 4H-$SrMnO_3$.

Figure 7 shows the specific heat of 6H-$SrMnO_3$, 4H-$SrMnO_3$, and C-$SrMnO_3$ at a zero magnetic field plotted as C_p/T vs T. There is no detectable difference in C_p at 0 and 70 kOe, indicating that a magnetic field (at least up to 70 kOe) has a very small effect on the AFM ordering. The characteristic peak (λ-type anomaly in the C_p vs T) was observed at 235 K for 6H-$SrMnO_3$ and C-$SrMnO_3$ and at 276 K for 4H-$SrMnO_3$, indicating the onset of long-range AFM ordering. A crossover feature is observed in the specific heat of three polymorphs near 90 K. The C_p of C-$SrMnO_3$ is smallest below $\sim$90 K but largest above $\sim$90 K (up to T_N). The C_p of 4H-$SrMnO_3$ is largest below $\sim$90 K but smallest above $\sim$90 K. This feature was emphasized and theoretically explained in Ref. 12. The C_p of 6H-$SrMnO_3$ lies between those of C-$SrMnO_3$ and 4H-$SrMnO_3$ in a wide temperature range.

Figure 8 shows electrical properties of 6H-$SrMnO_3$. The resistivity of 6H-$SrMnO_3$ is typical for semiconductors and follows the activation law $\rho = \rho_0 \exp(E_a/kT)$ with $E_a/k = 0.24$ eV.

IV. CONCLUSION

We investigated structural and magnetic properties of a previously unexplored polymorph of 6H-$SrMnO_3$. Compared with both C-$SrMnO_3$ and 4H-$SrMnO_3$ polymorphs, the magnetic properties of 6H-$SrMnO_3$ are closer to those expected for isotropic three-dimensional antiferromagnets. The T_N of 6H-$SrMnO_3$ is 235 K.

ACKNOWLEDGMENTS

This work was supported by World Premier International Research Center Initiative on Materials Nanoarchitectonics (Japan), by the NIMS Individual-Type Competitive Research Grant, by the Japan Society for the Promotion of Science (JSPS) through its Funding Program for World-Leading Innovative Research and Development on Science and Technology, and by grants-in-aid for scientific research (Grant Nos. 21540330 and 22246083) from JSPS. The synchrotron radiation experiments were performed at SPring-8 with the approval of the Japan Synchrotron Radiation Research Institute (Proposals No. 2009A4800 and No. 2009B4505).

*alexei.belik@nims.go.jp

[1] J. H. Lee and K. M. Rabe, Phys. Rev. Lett. **104**, 207204 (2010).

[2] S. Smadici, P. Abbamonte, A. Bhattacharya, X. F. Zhai, B. Jiang, A. Rusydi, J. N. Eckstein, S. D. Bader, and J. M. Zuo, Phys. Rev. Lett. **99**, 196404 (2007).

[3] I. D. Fawcett, J. E. Sunstrom, M. Greenblatt, M. Croft, and K. V. Ramanujachary, Chem. Mater. **10**, 3643 (1998).

[4] E. J. Cussen and P. D. Battle, Chem. Mater. **12**, 831 (2000).

[5] A. N. Christensen and G. Ollivier, J. Solid State Chem. **4**, 131 (1972).

[6]J. J. Adkin and M. A. Hayward, Chem. Mater. **19**, 755 (2007).
[7]J. J. Adkin and M. A. Hayward, J. Solid State Chem. **179**, 70 (2006).
[8]B. L. Chamberland, A. W. Sleight, and J. F. Weiher, J. Solid State Chem. **1**, 506 (1970).
[9]Y. Syono, S. I. Akimoto, and K. Kohn, J. Phys. Soc. Jpn. **26**, 993 (1969).
[10]K. Kuroda, N. Ishizawa, N. Mizutani, and M. Kato, J. Solid State Chem. **38**, 297 (1981).
[11]P. D. Battle, T. C. Gibb, and C. W. Jones, J. Solid State Chem. **74**, 60 (1988).
[12]R. Sondena, S. Stolen, P. Ravindran, and T. Grande, Phys. Rev. B **75**, 214307 (2007).
[13]R. Sondena, P. Ravindran, S. Stolen, T. Grande, and M. Hanfland, Phys. Rev. B **74**, 144102 (2006).
[14]H. Sakai, S. Ishiwata, D. Okuyama, A. Nakao, H. Nakao, Y. Murakami, Y. Taguchi, and Y. Tokura, Phys. Rev. B **82**, 180409 (2010).
[15]A. Sacchetti, M. Baldini, F. Crispoldi, P. Postorino, P. Dore, A. Nucara, C. Martin, and A. Maignan, Phys. Rev. B **72**, 172407 (2005).
[16]A. Daoud-Aladine, C. Martin, L. C. Chapon, M. Hervieu, K. S. Knight, M. Brunelli, and P. G. Radaelli, Phys. Rev. B **75**, 104417 (2007).
[17]R. Sondena, S. Stolen, P. Ravindran, T. Grande, and N. L. Allan, Phys. Rev. B **75**, 184105 (2007).
[18]L. S. Ramsdell, Am. Miner. **32**, 64 (1947).
[19]K. J. Lee and E. Iguchi, J. Solid State Chem. **114**, 242 (1995).
[20]T. Negas and R. S. Roth, J. Solid State Chem. **1**, 409 (1970).
[21]L. Suescun, O. Chmaissem, J. Mais, B. Dabrowski, and J. D. Jorgensen, J. Solid State Chem. **180**, 1698 (2007).
[22]M. Tanaka, Y. Katsuya, and A. Yamamoto, Rev. Sci. Instrum. **79**, 075106 (2008).
[23]F. Izumi and T. Ikeda, Mater. Sci. Forum **321-324**, 198 (2000).
[24]D. C. Sinclair, J. M. S. Skakle, F. D. Morrison, R. I. Smith, and T. P. Beales, J. Mater. Chem. **9**, 1327 (1999).
[25]R. E. Brese and M. O'Keeffe, Acta Crystallogr. B **47**, 192 (1991).